NUCLEAR THERMAL PROPULSION MATERIAL TRADE FOR ADDITIVELY MANUFACTURED REGENERATIVE CHAMBERS

Darren C. Tinker, Jackson Lusk, Paul Gradl

NASA Marshall Space Flight Center

Huntsville, Alabama

Nuclear thermal propulsion (NTP) is a game changing technology with advantages over chemical propulsion systems for deep space missions but comes with many engineering challenges. This paper focuses on the challenge of material selection for a regeneratively-cooled chamber for use in a nuclear environment with minimal design margins. Chemical compatibility with reactants and products following energy extraction (be it through combustion or neutron bombardment) must be considered. Similarly, mechanical and thermophysical properties (e.g., density, thermal conductivity, yield strength, etc.) as functions of temperature are critical. While hydrogen embrittlement environment (HEE) is a risk and consideration for traditional chemical combustion chambers, application in a nuclear thermal engine adds additional material compatibility and resilience requirements to long-term nuclear radiation exposure. Chamber materials in this trade included, but were not limited to, A-286, Haynes 230, Haynes 282, CRES 347, GRCop-42, GRCop-84, Inconel 625, JBK-75, and NASA HR-1. The material trade focuses on modern additive manufacturing techniques and hypothetical geometric constraints.

_____

INTRODUCTION

The highest-level constraint for the design process of a rocket engine is the mission objective. Once determined, vehicle designers set requirements for thrust class, geometric envelope, chamber pressure, minimum specific impulse, throat diameter, propellant section, and the target mixture ratio. These targets are flowed from engine systems models in the form of an initial power balance model (steady-state simulation of internal conditions and engine functions), engine requirements documents, interfaces across the engine, and component specific requirements such as life cycle, structural margins, maintenance, reliability.

The power balance model guides engine design and development, and its development is an iterative process with each of the component groups involved. A simplified example is shown in Figure 1 involving the combustion chamber and nozzle design on the component level. The power balance model will provide anticipated or target values for component performance (e.g., throat area, nozzle efficiency, allowable pressure budget (pressure drop across cooling channels), chamber pressure, mass-flow rates). Conceptual design cycles begin at the component level with these constraints and provide feedback where constraints or margins cannot be met. Under ideal circumstances, the power balance model iterates and flows down, updates, and flows feedback back up until a converging on an acceptable design solution. This design solution considers all disciplines of engineering and also studies the programmatic impacts such as cost, schedule, and various risks.

The material (metal alloy) selection of the chamber and nozzle is one of many decision points and, like all other components, has major impacts on engine functionality and reliability. Chemical compatibility with both reactants and products following energy extraction (be it through combustion or neutron bombardment) must be considered. Similarly, mechanical and thermophysical properties (e.g., chemistry, density, thermal conductivity, yield strength, elongation, etc.) as functions of temperature are critical. Higher strength materials often lead toward lower weight devices but come at the cost of lower thermal conductivity [1]. With all else constant, low conductivity inherently leads to higher temperatures. With rising temperatures, the yield strength of metals is reduced though exceptions do exist [2]. Superalloys are well-characterized for their high yield strength retention with temperature and have the highest strength-to-weight ratio.

While minimizing system mass is ideal, system constraints such as limited pressure loss, manufacturability, coolant mass flow rates, or chemical compatibility often limit options for the designer. If a high-strength, low-weight option is not possible due to violation of thermal or structural margins, a high-conductivity and (relatively speaking) higher density alternative must be considered. Modern engineering solutions to attain both high strength and high thermal conductivity include bimetallic designs where a thermally conductive metal is used to minimize hot-wall temperatures and is encased in a high-strength metal jacket [3]–[5].

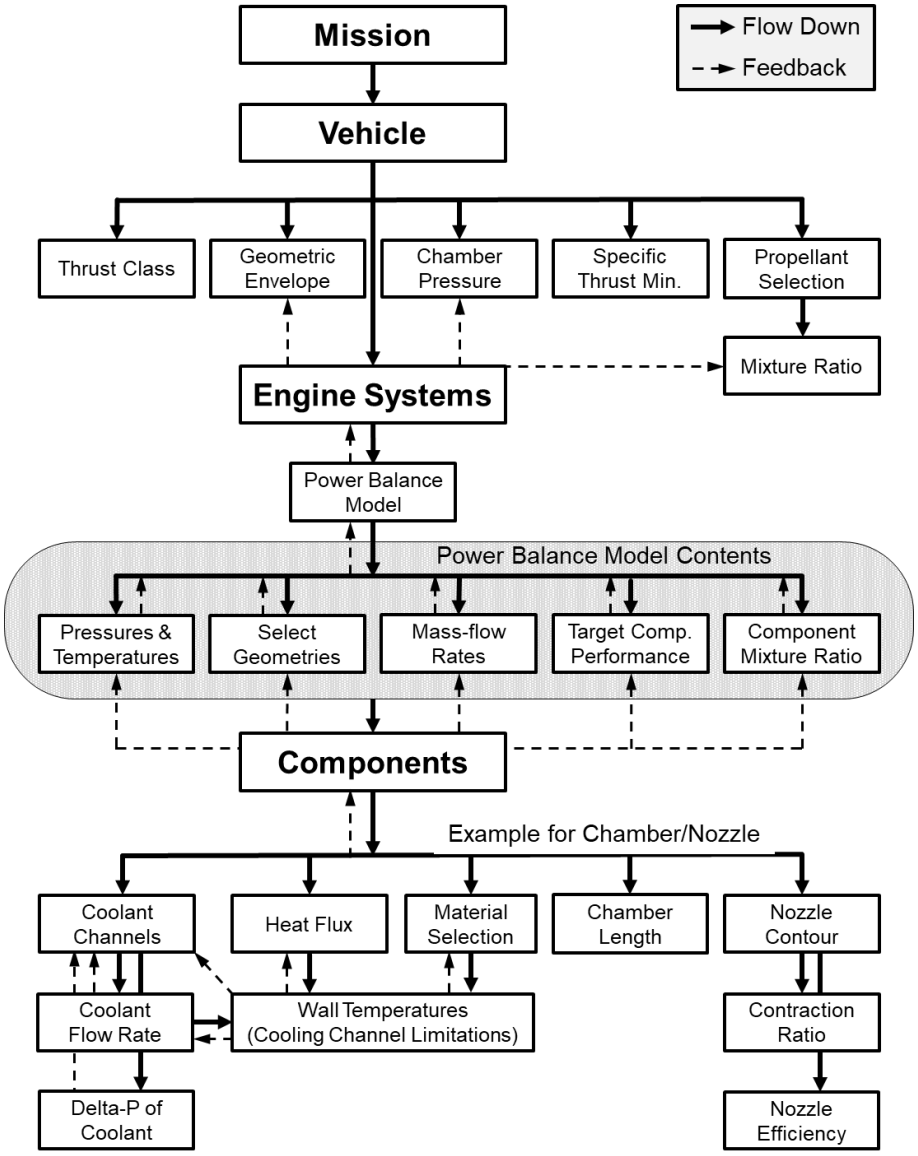

Figure 1 – Simplified flow down and feedback chart of requirements and targets for engine development.

MATERIAL TRADES

The chamber of a rocket engine must withstand high-temperature and high-pressure environments, which impose compounding stresses (axial, radial, including thrust loads) on the material. Appropriate mechanical and physical property selection are logically the key to success. Those primarily of interest for function are the alloy chemistry, yield and ultimate strength, thermal conductivity, ductility, low and high cycle fatigue life, corrosion, oxidation, and radiation resistance, fracture toughness, melting point, and thermal expansion [6]. Secondary interest applies to the material density for mass considerations as well as the hardness for manufacturability. Material composition is also important to determine compatibility with environmental factors (insensitivity to nuclear radiation) and both propellants and combustion products (resistance to embrittlement or oxidation).

A mission using a nuclear thermal propulsion (NTP) engine necessitates multiple duty cycles (starts and stops) during an interplanetary in-space flight and requires a design solution that does not rely on material or excess fuel consumption (i.e., ablative, film, or dump cooling). However, it is often the ground test requirements that drive the material and design limits since qualification requirements are often higher than flight. The thrust class and high-heat flux are not conducive to radiative cooling methods for the chamber (though this method is applicable to the nozzle extension to be joined). A regenerative cooling method is the resultant solution to meet mission needs and engine constraints, which often requires thin walls (<0.04 in., depending on the alloy) that must withstand extreme conditions. Further restricting design choices, the propellant for NTP will be pure, heated hydrogen requiring that the chamber be built from materials that are resilient to hydrogen embrittlement environment (HEE) [7].

Modern fabrication methods of aerospace combustion devices have trended toward the use of additive manufacturing due to advantages in complexity, part consolidation, and cost and schedule economics [3], [5], [8], [9]. The continually maturing field is now able to print a various metal alloy families [8], [10]–[13], superalloys [6], [14], [15], copper alloys [3] and bimetallic structures [3], [5], [16], [17] that were previously unavailable, or extremely challenging, as design solutions though additive manufacturing methods. The availability of AM data and uncertainty in properties for newer alloys call for trade studies to discuss and outline the potential benefits for future use.

Yield Strength

A selection of materials used for previously manufactured combustion chambers were considered as design solutions. The yield strengths at ambient temperature varied from 20 ksi up to 140 ksi as shown in Figure 2. Super alloys examined here – A-286, Haynes 230, Haynes 282, Inconel 625, JBK-75, and NASA HR-1 – were initially determined for with an average room temperature yield strength from 50 to 140 ksi, which are 2-5x greater than the ferrous and copper-based alloys (347 SS, GRCop-42, and GRCop-84). These values are for wrought material properties and mechanical properties for AM parts are anticipated to vary

The relative decrease in yield strength with rising temperature (up to ~1,600 R) is much lower for superalloys, which is the cornerstone of their performance characteristics (others being resistance to creep and corrosion) [18]. The superalloys examined maintained anywhere from 70-90% of their ambient yield strength up to 1600 R (890 K). Ferrous and copper-based alloys alternatively range between 50-60% of ambient superalloy yield strength at the same point with sharper drop offs as the melting temperatures were approached. The resultant differences between superalloys and other metal alloy strengths at high temperatures increased from factors of 2-5 to 3-10 times greater in value. However, chambers rarely fail in a nominal condition and off-nominal considerations need to be considered including streaking, high heat fluxes, variations in manufacturing, variation in properties and a material should not operate at the peak limit with nominal design conditions.

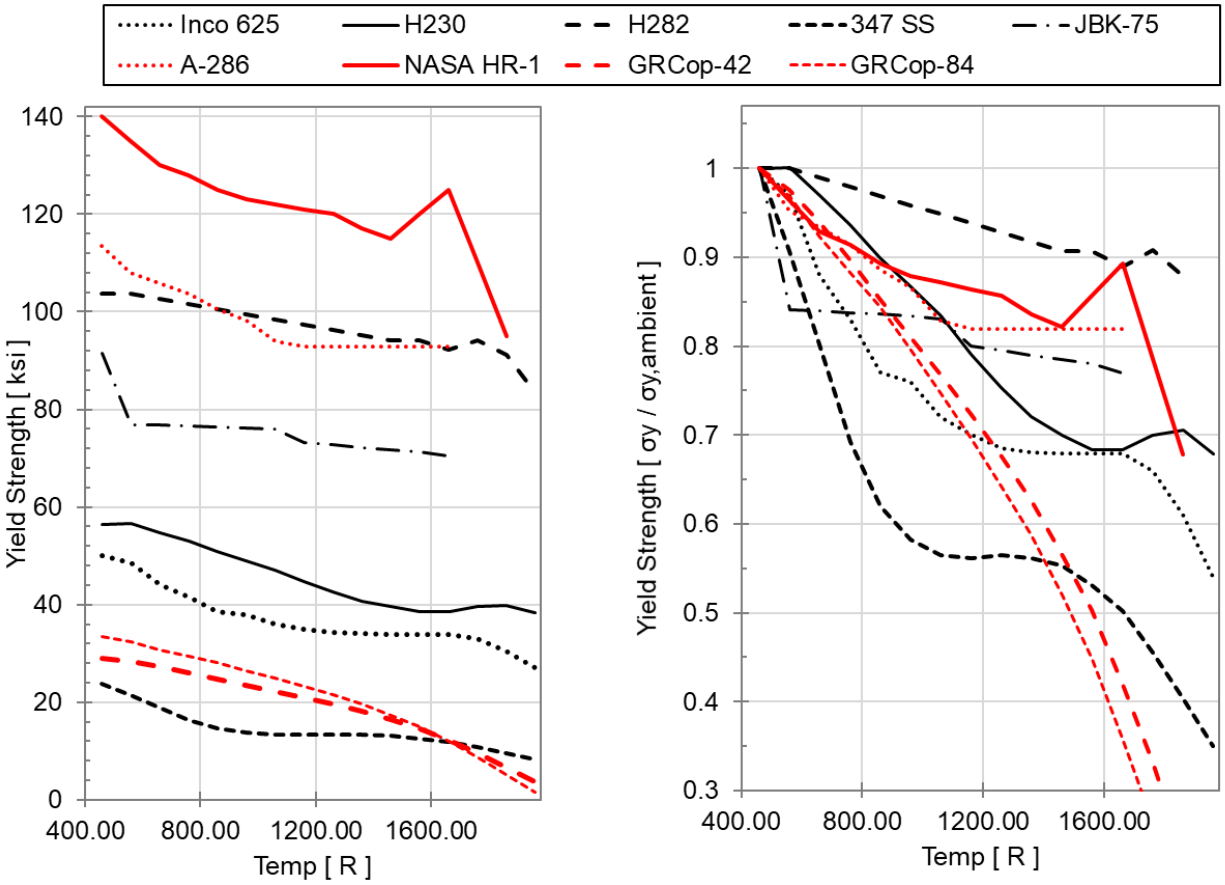

Figure 2 – Yield strength (ksi, left; percent ambient yield, right) vs. temperature [13],[19],[20],[21],[22],[23],[24],[26].

Thermal Conductivity

If held at similar temperatures, superalloys offer higher structural margin than their existing ferrous and copper-based alloy counterparts. Due diligence therefore demands investigation of thermal properties (e.g., thermal conductivity, thermal expansion, and melting points) to appropriately assess design solutions since chambers are at their core a heat exchanger.

When discounting azimuthal or axial cooling effects (i.e., reducing to one dimension), heat flux into the chamber is predominately due to convective heat transfer as described by Equation 1 and shown by Figure 3,

$$q = h_g(T_{aw} - T_{wg}) \quad [1]$$

where q is heat flux transferred across the stagnant gas film per unit area, h_g is the convective heat transfer coefficient of the fluid, T_{aw} is the adiabatic wall temperature of the gas, and T_{wg} is the temperature of the hot-gas-side of the chamber wall. Explicitly, all values must be discretized for analysis with practical application as the wall temperatures and convective coefficient will vary due to localized conditions.

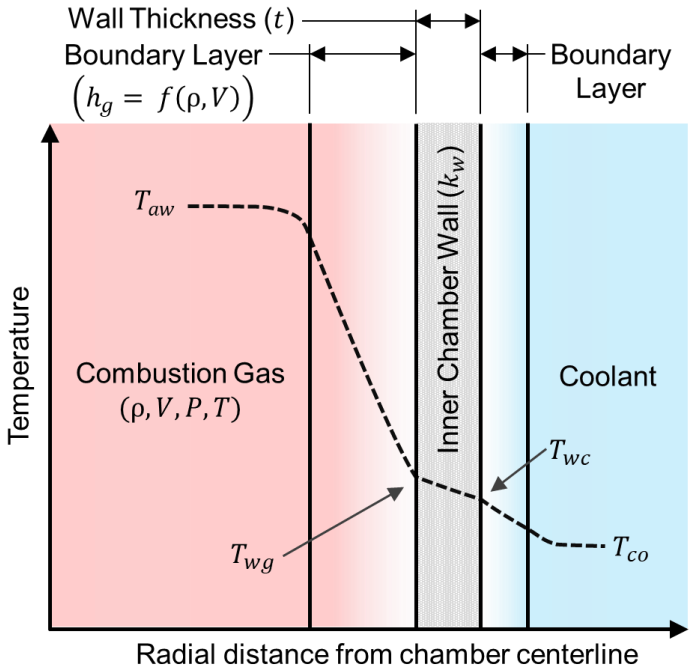

Figure 3 – Schematic of 1D heat transfer model for regenerative cooling.

An equivalent amount of heat must be dissipated from the part and occurs through conductive transfer to a coolant fluid on the opposing wall as shown in Equation 2,

$$q = \frac{k_w}{t}(T_{wg} - T_{wc}) \quad [2]$$

where k_w is the thermal conductivity of the wall, t is the wall thickness, and T_{wc} is the coolant-side wall temperature. Through substitution and algebraic manipulation results in Equation 3. that may be used to calculate a local hot-wall temperature.

$$T_{wg} = \frac{\left(T_{aw} + T_{wc} * \frac{k_W}{h_g t}\right)}{\left(\frac{k_w}{h_g t} + 1\right)} \quad [3]$$

The unknowns in this equation are the (1) coolant-wall temperatures, (2) fluid temperature, (3) wall thermal conductivity, (4) fluid convective coefficient, and the (5) wall thickness. For the sake of the material trade, temperatures and wall thicknesses are assumed uniform for all cases. To ensure a conservative estimate for the hot wall temperature, the coolant wall temperature (T_{wc}) at the throat is assumed to be 500 R and the adiabatic wall temperature (T_{aw}) is assumed to be 4500 R. The adiabatic wall temperature is calculated from assuming a chamber temperature (T_0) of 5000 R and 0.90 for the effective recovery factor [25]. The hot-wall thickness (t) is assumed uniform for all materials at 0.040 inches.

The reader must consider that this calculation assumes ideal heat transfer where the cold wall is equal to the coolant temperature. This requires a high convective heat transfer coefficient of the coolant fluid, which may be limited due to practical constraints of geometric limits, surface finishes, and fluid velocities. Furthermore, the fluid temperature will be dependent on heat loads prior to reaching the throat. This will result in an increased coolant temperature, further reducing the cooling potential.

With three of the five unknowns eliminated by constant-value assumptions, the thermal conductivity is determined by material properties studied here. Figure 4 shows the relation of thermal conductivities versus temperature for superalloys and ferrous-based alloys. Typically, higher strength materials have lower thermal conductivities, but half of the super alloys (A-286, Haynes 2xx, JBK-75, and NASA HR-1) have comparable thermal conductivities to stainless steel 347, which has one fifth of the strength if not less. Without any further analysis, this ferrous-based alloy (SS 347) as well as a similarly performing Inconel 625 are not optimal material selections.

Expanding to include copper-based alloys, Figure 5 displays the thermal conductivity and elongation for all the materials of interest. Elongation (ductility) is comparable for all materials and an important consideration due to cyclic thermal loading. For example, a ceramic or composite could offer extremely high strengths, yet have low ductility and fail due to the fully reversal loads (compressive to tensile) across a short distance burdened with a sharp thermal gradient – one that ranges from near zero cryogenic temperatures to a few thousand Rankine.

When evaluating thermal conductivity, in sharp contrast to Figure 2, copper-based alloys show a markedly higher performance than their superalloy and ferrous alloy competitors. As typically observed for metals and metal alloys, an inverse relation of strength and conductivity exists. However, the magnitude of difference (a factor of 20) is substantial. Data for ambient conditions is consolidated into Table 1 below.

Table 1 – Material properties at ambient conditions

Property	Unit	A-286	GRCop-42	GRCop-84	Inco 625	HR-1	H230	H282	JBK-75	347 SS
Yield	ksi	108	25	23	50	137	60	102	77	30
Ultimate	ksi	160	48	55	110	183	121	165	145	75
Elongation	%	26	32	29	50	24	47	30	29	40
Conductivity at 560 R	BTU / hr-ft-R	7.33	219	144	6.3	7.11	5.17	7.3	9	9.3
Source	[-]	[19]	[13]	[20]	[19]	[21]	[22]	[23]	[24]	[19], [26]

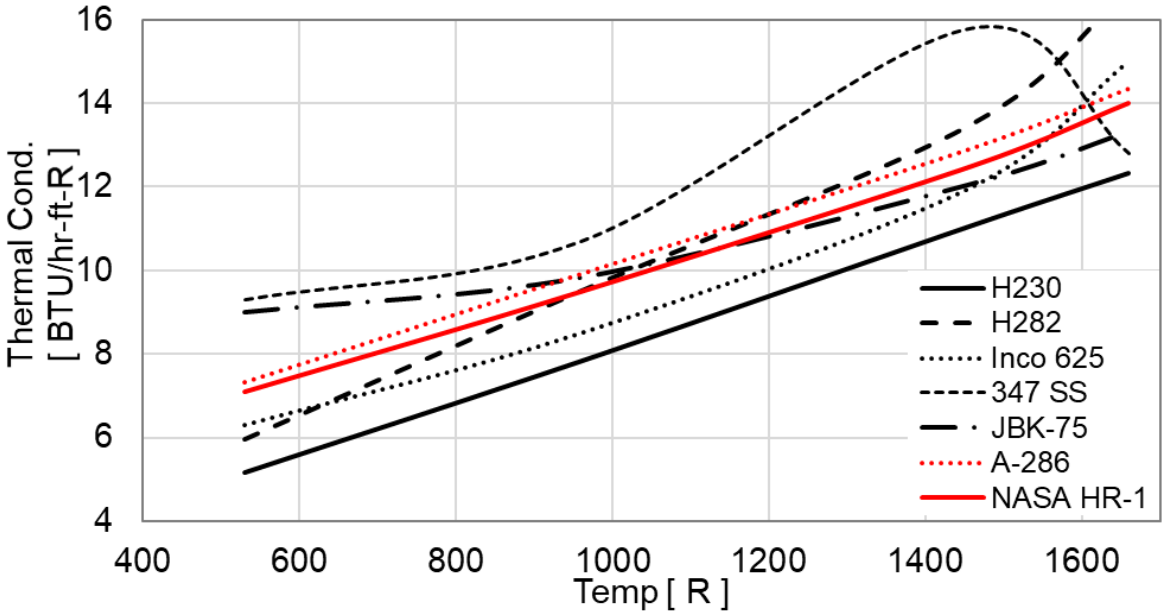

Figure 4 – Thermal conductivities of superalloy and ferrous-based alloys.

(U)

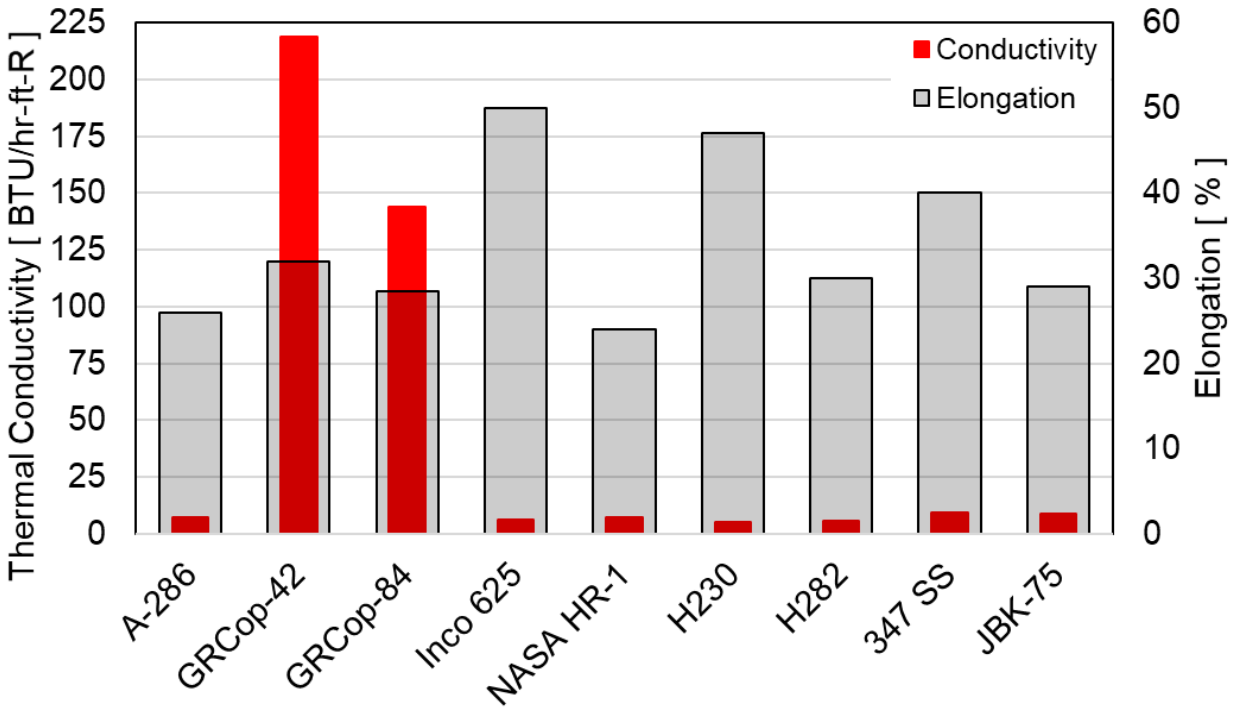

Figure 5 – Thermal conductivity and elongation percentage per trade study material.

The convective heat transfer coefficient is calculated through the Bartz equation [25], [27], [28] as shown below in Equation 4,

$$h_g = \left[\frac{0.026}{D_t^{0.2}}\left(\frac{\mu^{0.2}C_p}{Pr^{0.6}}\right)_{ns}\left(\frac{(Pc)_{ns} * g}{c^*}\right)^{0.8}\left(\frac{D_t}{R}\right)^{0.1}\right] * \left(\frac{A_t}{A_{local}}\right)^{0.9} * \sigma \quad [4]$$

$$\text{Where } \sigma = \frac{1}{\left[\frac{1}{2}*\frac{T_{wg}}{(Tc)_{ns}}*\left(1+\frac{\gamma-1}{2}M^2\right)+\frac{1}{2}\right]^{0.68} * \left[1+\frac{\gamma-1}{2}M^2\right]^{0.12}} \quad [5]$$

where Dt is the throat diameter, μ the viscosity (chemically frozen), C_p is the specific heat (chemically frozen), Pr is the Prandtl number, Pc is the chamber pressure, g is the gravitational constant, $c*$ is the characteristic velocity, R is the converging convex radius of the chamber contour at the throat, At is the throat area, A is the local area, T_{wg} is the local hot wall temperature, T_c is the chamber temperature, γ is the specific heat ratio (chemically frozen), M is the Mach number, and the subscript ns denotes chamber stagnation properties.

A sample chamber design is presented in Figure 6 with the normalized temperatures, pressures, and densities; local Mach numbers; and convective heat transfer coefficient as calculated by Equation 4. The local maximum is found just before the throat as primarily driven by the contraction ratio. From this method, the peak convective heat transfer coefficient is 0.0135 BTU/in^2-s-R.

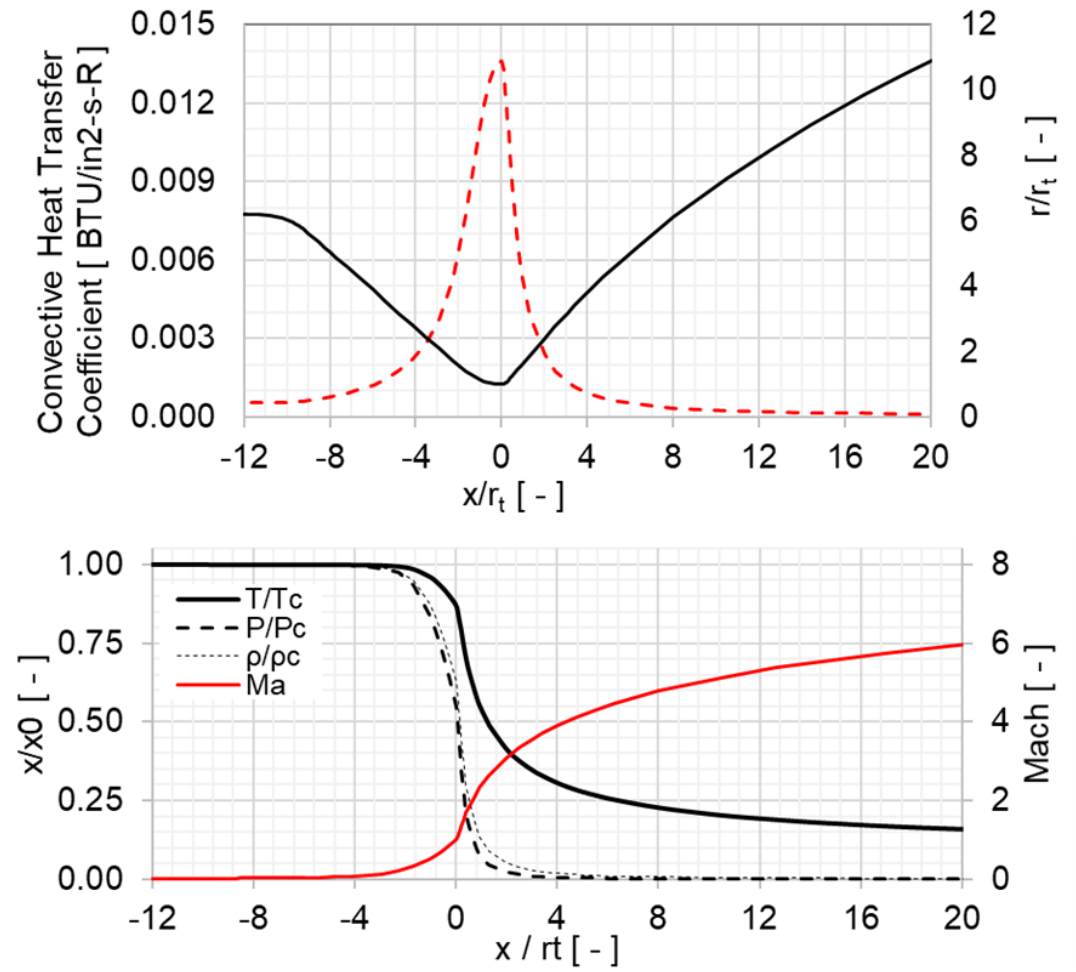

Figure 6 – Sample nozzle geometry and resultant gas dynamic calculations.

Returning to Equation 3, a first pass of hot-wall temperatures may be calculated. The results are presented in Table 2 as well as the thermal-structural margin (50% of the melting temperature) as defined by Equation 6,

$$Margin = 1 - \frac{T_{calc}}{50\% * T_{melt}} \quad [6]$$

GRCop alloys had the highest margin, followed by JBK-75 and 347 SS. All other superalloys performed similarly with margins between 25 to 36%. Haynes 230 was predicted to have the worst performance, and GRCop-42 was predicted to have the best. GRCop alloys were estimated to maintain wall temperatures at almost half the value of the nearest non-copper alloy. Recalling that 347 SS has similar strength to GRCop alloys, the operating temperature is a key comparator for yield strengths.

Since superalloys have similar thermal performance and thermal-structural margins, the relative yield strength becomes the driving factor. NASA HR-1 is over 10% greater in strength than the next closest material (Haynes 282). All ferrous and superalloys are expected to maintain similar operating temperatures, and consequently NASA HR-1 appears to be the best option.

Table 2 – First-order results for hot wall temperature, melting temperature, and thermal-structural margin.

Property	Unit	A-286	GRCop-42	GRCop-84	Inco 625	NASA HR-1	H230	H282	JBK-75	347 SS
T_{wg}	R	1023	538	551	1058	1038	1097	1004	938	959
T_{melt}	R	3000	2400	2400	2810	2885	2910	2830	2959	3010
Thermal-Structural Margin	[-]	32%	43%	37%	25%	28%	25%	29%	37%	36%

Radiation and Hydrogen Embrittlement

Before delving into effects of radiation, the general question of hydrogen compatibility may be addressed. A thorough review of existing studies was consolidated by Lee [7] and relevant materials are presented in Table 3. A negligible or small rating permits use within the specified testing range. A high rating advises limited use, and a severe rating is not advised for use. Full details may be found in NASA/TM-2016–218602 [7]. The only severe rating is listed for A-286 that is both solution treated and aged. Inconel 625 and Haynes 230 were rated high. The materials of least concern for hydrogen compatibility are solution treated A-286, GRCop-84, NASA HR-1, and 347 Stainless Steel.

Table 3 – Hydrogen embrittlement ratings for candidate materials.

Material	Qualitative Rating for Hydrogen Environmental Embrittlement
A-286	Negligible, Severe (w/Aging) [7]
GRCop-42	Not Available
GRCop-84	Negligible [7], [29]
Inco 625	High [7], [30]
JBK-75	Negligible, High (w/ST + Aging) [7]
NASA HR-1	Negligible (Small) [7], [21], [31]
H230	High [7]
H282	Not Available, but assumed high since Ni-based
347 SS	Small [7], [32]

Two materials (GRCop-42 and Haynes 282) did not have data available and were considered equivalent to their counterparts – GRCop-84 and Haynes 230, respectively. Material compositions were analyzed to predict potential impacts as shown in Table 4. GRCop-84 and GRCop-42 both have a ratio of 1.14:1, Cr:Nb. The ratio of copper to chromium and niobium is the key difference but is not anticipated to cause issue as pure copper has negligible risk itself [7]. Existing literature discusses concerns of hydrogen isotope absorption by niobium leading to embrittlement, but the occurrence is extremely low with the presence of Cr_2Nb and a slight excess of chromium [33]. Differences between Haynes 230 and Haynes 282 are not as straightforward (i.e., substitution instead of a composition shift). In Haynes 282, the equivalent percentage of tungsten from Haynes 230 is replaced with part cobalt and part molybdenum. This change is not anticipated to shift the risk of hydrogen embrittlement, but a metallurgical evaluation from a subject matter expert is warranted prior to selection.

To further complicate matters, the hydrogen propellant is energized by a reactor core. The fluid is anticipated to enter the main chamber in a supercritical or gaseous state with an increased presence of both ionized species and radioactive isotopes (tritium and deuterium). The reactions altering gaseous hydrogen from its equilibrium state (a ratio of para- to orthohydrogen as a function of temperature) are not spontaneous, and require an energy source for the mechanism to progress [34]. The activation energy provided in this application is both gamma and neutron radiation from the reactor core, which is based on a low-enriched uranium (<20% U-235) fission reaction [35]. The question of “what quantity of nonequilibrium species” are created is a question of residence time within the reactor and requires a separate and detailed

study. For this analysis, the assumption is that these ionized and radioactive species may be present in a non-negligible quantity.

The concern of radioactive isotopes, ionized hydrogen, and general embrittlement is not limited to the hot wall of the regenerative chamber, but also supercritical and gaseous propellants in the cooling channels. Conversion from para- to ortho-states is primarily of interest due to the enthalpy difference, where the ortho-state is lower than that of parahydrogen. This has potential negative impacts on both the turbomachinery and regenerative chamber where energy conversion occurs. The impact on turbomachinery is limited to the turbine as the pump operates at liquid temperatures. Cryogenic hydrogen (found at the inlet of the chamber and preceding hardware to the tank) is susceptible to both gamma and neutron radiation that escapes the reactor core, but has near zero conversion at liquid hydrogen temperatures [36]. Therefore, the concerns are limited to system components inclusive and downstream of the regenerative channels, the reactor core cooling channels, and potentially cryogenic fluid management systems.

While mechanical properties of metals are resilient to gamma radiation and are often used as radiation shields, the material selection may still affect the propellant. As an example, stainless steels act as a catalyst for conversion from parahydrogen to orthohydrogen and long-duration, low-flux radiation has a greater effect on conversion than short-duration, high-flux radiation [36]. Such a study is out of scope for the needs of the regenerative chamber due to low residence times (milliseconds whereas the catalytic conversion occurs on the order of minutes or hours [37]) but should be considered on a system level analysis.

Table 4 – Material Compositions [19]–[21]**.**

		Al	B	C	Co	Cr	Cu	Fe	La	Mn	Mo	Nb	Ni	P	S	Si	Ti	Va	W	Other
A-286	Min	-	0.003	-	-	13.500	-	Bal.	-	-	1.000	-	24.000	-	-	-	1.900	0.100	-	0.030
	Nominal	0.175	0.007	0.040	-	14.750	-	50.410	-	0.175	1.250	-	25.500	0.013	0.013	0.500	2.125	0.300	-	0.215
	Max	0.350	0.010	0.080	-	16.000	-	Bal.	-	0.350	1.500	-	27.000	0.025	0.025	1.000	2.350	0.500	-	0.400
JBK-75	Min	-	-	0.020	-	14.500	-	Bal.	-	0.110	1.220	-	29.500	-	-		1.850	-	-	-
	Nominal	0.135	0.001	0.022	-	14.850	-	49.774	-	0.150	1.375	-	30.000	0.006	0.005	0.085	1.960	0.125	-	-
	Max	0.270	0.001	0.024	-	15.200	-	Bal.	-	0.190	1.530	-	30.500	0.011	0.010	0.170	2.070	0.250	-	-
GRCop-42	Min	-	-	-	-	3.100	Bal.	-	-	-	-	2.700	-	-	-	-	-	-	-	-
	Nominal	-	-	-	-	3.250	93.600	-	-	-	-	2.850	-	-	-	-	-	-	-	-
	Max	<50 ppm	-	-	-	3.400	Bal.	<50 ppm	-	-	-	3.000	-	-	-	<50 ppm	-	-	-	<400 ppm
GRCop-84	Min	-	-	-	-	6.200	Bal.	-	-	-	-	5.400	-	-	-	-	-	-	-	-
	Nominal	-	-	-	-	6.500	87.200	-	-	-	-	5.700	-	-	-	-	-	-	-	-
	Max	<50 ppm	-	-	-	6.800	Bal.	<50 ppm	-	-	-	6.000	-	-	-	<50 ppm	-	-	-	<400 ppm
NASA HR-1	Min	0.200	-	-	3.000	14.000	-	29.000	-	-	1.800	-	33.000	-	-	-	2.500	0.300	1.500	-
	Nominal	0.250	-	0.005	3.250	15.000	-	31.000	-	-	2.000	-	34.000	0.003	0.003	0.025	2.600	0.400	1.750	-
	Max	0.300	-	0.010	3.500	16.000	-	33.000	-	-	2.200	-	35.000	0.005	0.005	0.050	2.700	0.500	2.000	-
Haynes 230	Min	0.200	-	0.050	-	20.000	-	-	0.005	0.300	1.000	-	Bal.	-	-	0.250	-	-	13.000	-
	Nominal	0.350	0.008	0.100	2.500	22.000	0.250	1.500	0.028	0.650	2.000	0.250	9.715	0.015	0.008	0.500	0.050	-	14.000	-
	Max	0.500	0.015	0.150	5.000	24.000	0.500	3.000	0.050	1.000	3.000	0.500	57.000	0.030	0.015	0.750	0.100	-	15.000	-
Haynes 282	Min	1.380	0.003	0.040	9.000	18.500	-	-	0.005	-	8.000	-	Bal.	-	-	-	1.900	-	13.000	0.020
	Nominal	1.515	0.007	0.060	10.000	19.500	0.050	0.750	-	0.150	8.500	-	9.715	0.008	0.008	0.075	2.100	-	-	0.020
	Max	1.650	0.010	0.080	11.000	20.500	0.100	1.500	-	0.300	9.000	-	57.000	0.015	0.015	0.150	2.300	-	-	0.020
347 SS	Min	-	-	0.040	-	17.000	-	Bal.	-	2.000	-	0.035	9.000	0.045	0.030	0.750	1.900	-	-	-
	Nominal	-	-	0.070	-	18.000	-	61.775	-	2.000	-	0.518	11.000	0.045	0.030	0.750	2.100	-	-	-
	Max	-	-	0.100	-	19.000	-	-	-	2.000	-	1.000	13.000	0.045	0.030	0.750	2.300	-	-	-

MANUFACTURING CONSIDERATIONS

The state of modern manufacturing must be considered for each material. Chambers and nozzles are large components that have traditionally been formed by series of tubes, milled channels with specialized joining process for closeout, and more recently, additively manufactured channels [38], [39]. Additive manufacturing methods are known best for the ability to create complex geometry that would otherwise be impossible to machine using subtractive techniques. A lesser sung benefit is the rapid production time in comparison.

Powder bed methods, such as laser powder bed fusion (L-PBF), are capable of much finer resolution yet are restricted to small build boxes and are presently impractical for creating large parts (>15” diameter) [40]. Producing large parts relies on freeform additive manufacturing methods and related hybrid technologies such as Direct Metal Deposition (DMD or blown powder deposition); Wire-based laser deposition; Laser Powder Directed Energy Deposition (LP-DED); Arc-based wire deposition; or Electron Beam Freeform Fabrication (EBF^3). However, each of these techniques are not equal and only a few are capable of finer resolution channels.

While most of these alloys have been used in L-PBF AM and can build functional parts, there are far less candidates that have been used for freeform additive techniques. Development and maturation of these AM processes require full process and alloy maturation. Consequently, they are restricted to traditional manufacturing techniques, which are time-intensive in comparison to additive methods. Table 5 outlines the candidate materials and what processes have been matured for each [40]. Starred markings have been tested in an academic setting but are not available through commercial service vendors.

Those not marked “as-demonstrated” with LP-DED methods are not eligible materials as they cannot produce parts of sufficient size (A-286, Haynes 282, 347 SS). While 347 SS may be used to create an external liner for a chamber or nozzle with integrated channels (as can Inconel 625, NASA HR-1, Haynes 230, and JBK-75), it presently is not a method that can be standalone to produce the part in a single manufacturing process. Given the higher thermal conductivity and comparable strength to materials such as 347 SS, it is anticipated that GRCop alloys will meet structural requirements.

Table 5 – Demonstrated additive manufacturing techniques per material.

Method	A-286	GRCop-42	GRCop-84	Inco 625	NASA HR-1	H230	H282	JBK-75	347 SS
L-PBF		x	x	x	x	x	x	x	x*
Laser Wire Direct Closeout				x	x	x		x	x
LP-DED		x	x	x	x	x		x	
Source		[3], [41]	[3], [41]	[42]	[42]	[7], [43]		[41], [42]	[41], [44]

CONCLUSION

A trade study for the regenerative chamber material selection was performed. NASA HR-1 and GRCop-42 were selected as candidate materials moving forward. The decision to pursue GRCop-42 and NASA HR-1 as potential alloys is motivated not only by sound engineering principles and risk reduction, but also the ability to advance the present state of the field for manufacturing processes.

As calculated with an unrefined, one-dimensional heat transfer analysis, the material with the best thermal performance was GRCop-42. Despite GRCop-42 having a lower yield strength than superalloys and its ferrous-based competitors, the thermal conductivity being twenty times greater cannot be excluded as a design solution that will meet both structural and thermal margins – consequently, GRCop-42 is a reasonable candidate material.

Haynes 230, Haynes 282, and Inconel 625 were discounted due to risks of hydrogen embrittlement. While these materials may be used under specified ranges, the operating temperatures and pressures of the nuclear thermal engine present an unknown regime and therefore unacceptable risk without extensive testing. Stainless steel 347 had a small risk of embrittlement, but not enough to warrant elimination. It is instead eliminated due to (1) its low yield strength relative to other materials with comparable thermal conductivity and (2) low thermal conductivity relative to materials with comparable yield strength. In addition to concerns of embrittlement and comparative mechanical properties, A-286, Haynes 282, and 347 SS are not ideal candidates due to the desire for risk reduction through additive manufacturing methods and maturation for each material.

Non-copper alloys have much lower thermal performance. While other superalloys and ferrous-based alloys had similar thermal margins, NASA HR-1 remains as the optimal choice due to a 15-40% greater yield strength (up to 230% greater if including Inconel 625) across all temperature ranges. Due to the comparable thermal performance and significantly higher structural performance, NASA HR-1 is considered the second candidate material.

A continuum of design solutions exists. Within that, there are countless that satisfy operational requirements using the materials selected in this trade study as well as those that were eliminated. Cost of each material has not been compared and total system mass was not considered. The analysis presented here is a first-order, rudimentary approach that does not consider the effects of radiation cooling, complex fluid dynamics, off-nominal conditions (e.g., uneven heat distribution, streaking, nonuniform flow). More advanced approaches will yield more realistic results, with experimental data providing necessary validation.

ACKNOWLEDGMENTS

This work was funded by the NASA Space Nuclear Propulsion program.

REFERENCES

[1] M. F. Ashby, *Materials Selection in Mechanical Design*, 5th ed. Cambridge: Butterworth-Heinemann, 2017.

[2] R. E. Smallman, *Modern Physical Metallurgy*. London: Elsevier Science, 1985.

[3] P. R. Gradl, C. S. Protz, D. L. Ellis, S. E. Greene, and B. P. Road, “Progress in Additively Manufactured Copper-Alloy GRCop-84 , GRCop-42 , and Bimetallic Combustion Chambers for Liquid Rocket Engines,” in *International Astronautical Congress (IAC)*, 2019, no. October, pp. 21–25, [Online]. Available: https://ntrs.nasa.gov/citations/20190033311.

[4] F. Kerstens, A. Cervone, and P. Gradl, “End to end process evaluation for additively manufactured liquid rocket engine thrust chambers,” *Acta Astronaut.*, vol. 182, no. February, pp. 454–465, May 2021, doi: 10.1016/j.actaastro.2021.02.034.

[5] P. R. Gradl, C. Protz, S. E. Greene, D. Ellis, B. Lerch, and I. Locci, “Development and Hot-fire Testing of Additively Manufactured Copper Combustion Chambers for Liquid Rocket Engine Applications,” in *53rd AIAA/SAE/ASEE Joint Propulsion Conference*, Jul. 2017, pp. 1–27, doi: 10.2514/6.2017-4670.

[6] C. Katsarelis *et al.*, “Additive Manufacturing of NASA HR-1 Material for Liquid Rocket Engine Component

Applications," in *JANNAF*, 2019, pp. 1–15.

[7] J. A. Lee, "Hydrogen Embrittlement," NASA/TM-2016–218602, Huntsville, NASA/TM-2016–218602 Hydrogen, 2016.

[8] R. P. Minneci, E. A. Lass, J. R. Bunn, H. Choo, and J. Claudia, "Copper-based alloys for structural high-heat-flux applications : a review of development , properties , and performance of Cu-rich Cu – Cr – Nb alloys development , properties , and performance of Cu-rich Cu – Cr – Nb alloys," *Int. Mater. Rev.*, vol. 0, no. 0, pp. 1–32, 2020, doi: 10.1080/09506608.2020.1821485.

[9] C. S. Protz *et al.*, "Large-Scale Lightweight Composite Overwrap Combustion Chambers and Nozzles under the Rapid Analyiss and Manufacturing Propulsion Technology (RAMPT Project)," in *JANNAF 11th Liquid Propulsion Subcommittee (LPS)*, 2019, pp. 1–46.

[10] S. L. Sing and W. Y. Yeong, "Laser powder bed fusion for metal additive manufacturing: perspectives on recent developments," *Virtual Phys. Prototyp.*, vol. 15, no. 3, pp. 359–370, Jul. 2020, doi: 10.1080/17452759.2020.1779999.

[11] T. A. Bars, M. Products, A. Rivets, C. Wire, and N. R. A. Products, "Standard Guide for Evaluating Mechanical Properties of Metal Materials Made via Additive Manufacturing Processes 1," pp. 1–6, 2020, doi: 10.1520/F3122-14.2.

[12] W. S. Gora *et al.*, "Enhancing Surface Finish of Additively Manufactured Titanium and Cobalt Chrome Elements Using Laser Based Finishing," *Phys. Procedia*, vol. 83, pp. 258–263, 2016, doi: 10.1016/j.phpro.2016.08.021.

[13] P. R. Gradl, C. S. Protz, K. Cooper, D. Ellis, L. J. Evans, and C. Garcia, "GRCop-42 Development and Hot-fire Testing Using Additive Manufacturing Powder Bed Fusion for Channel-cooled Combustion Chambers," in *AIAA Propulsion and Energy 2019 Forum*, Aug. 2019, vol. 1, pp. 1–26, doi: 10.2514/6.2019-4228.

[14] Z. Wu, S. P. Narra, and A. Rollett, "Exploring the fabrication limits of thin-wall structures in a laser powder bed fusion process," *Int. J. Adv. Manuf. Technol.*, vol. 110, no. 1–2, pp. 191–207, 2020, doi: 10.1007/s00170-020-05827-4.

[15] P. R. Gradl, C. S. Protz, and T. Wammen, "Additive Manufacturing and Hot-fire Testing of Liquid Rocket Channel Wall Nozzles Using Blown Powder Directed Energy Deposition Inconel 625 and JBK-75 Alloys," in *AIAA Propulsion and Energy 2019 Forum*, Aug. 2019, vol. AIAA-2019-, pp. 1–20, doi: 10.2514/6.2019-4362.

[16] P. R. Gradl, C. S. Protz, K. Zagorski, V. Doshi, and H. McCallum, "Additive Manufacturing and Hot-fire Testing of Bimetallic GRCop-84 and C-18150 Channel-Cooled Combustion Chambers Using Powder Bed Fusion and Inconel 625 Hybrid Directed Energy Deposition," in *AIAA Propulsion and Energy 2019 Forum*, Aug. 2019, vol. 2019, pp. 1–12, doi: 10.2514/6.2019-4390.

[17] P. R. Gradl, S. Greene, and T. Wammen, "Bimetallic Channel Wall Nozzle Development and Hot-fire Testing Using Additively Manufactured Laser Wire Direct Closeout Technology," in *AIAA Propulsion and Energy 2019 Forum*, Aug. 2019, no. August, pp. 1–18, doi: 10.2514/6.2019-4361.

[18] C. T. Sims, "A History of Superalloy Metallurgy for Superalloy Metallurgists," in *Superalloys 1984 (Fifth International Symposium)*, 1984, pp. 399–419, doi: 10.7449/1984/Superalloys_1984_399_419.

[19] *Metallic Materials Properties Development and Standardization (MMPDS) Handbook - 14*, 15th ed. Columbus: Battelle Memorial Institute, 2020.

[20] D. L. Ellis, "GRCop-84 : A High-Temperature Copper Alloy for High-Heat-Flux Applications," Cleveland, Ohio, 2005. [Online]. Available: https://ntrs.nasa.gov/citations/20050123582.

[21] P. S. Chen, B. Panda, and B. N. Bhat, "NASA-HR-1, A New Hydrogen-Resistant Fe-Ni-Base Superalloy," in

Hydrogen Effects in Materials, no. April, Hoboken, NJ, USA: John Wiley & Sons, Inc., 2013, pp. 1011–1020.

[22] "Haynes International - Haynes 230 Principal Features," 2020. https://www.haynesintl.com/alloys/alloy-portfolio_/High-temperature-Alloys/HAYNES-230-ALLOY.aspx.

[23] "Haynes International - Haynes 282 Principal Features," 2020. https://www.haynesintl.com/alloys/alloy-portfolio_/High-temperature-Alloys/HAYNES282alloy.aspx.

[24] "DED JBK-75 Mechanical Test Data," *NASA MSFC, Unpubl. results*, 2020.

[25] D. H. Huang and D. K. Huzel, *Modern Engineering for Design of Liquid-Propellant Rocket Engines*, 2nd ed. Washington DC: American Institute of Aeronautics and Astronautics, 1992.

[26] "HIGH-TEMPERATURE CHARACTERISTICS OF STAINLESS STEELS," Nickel Development Institute, 2020.

[27] D. R. Bartz, "Technical Notes," *J. Jet Propuls.*, vol. 27, no. 1, pp. 49–53, Jan. 1957, doi: 10.2514/8.12572.

[28] D. R. Bartz, "An Approximate Solution of Compressible Turbulent Boundary-Layer Development and Convective Heat Transfer in Convergent-Divergent Nozzles," *J. Fluids Eng.*, vol. 77, no. 8, pp. 1235–1244, Nov. 1955, doi: 10.1115/1.4014652.

[29] D. L. Ellis, A. K. Misra, and R. L. Dreshfield, "Effect of Hydrogen Exposure on a Cu-8 Cr-4 Nb Alloy for Rocket Motor Applications," in *Hydrogen Effects in Materials*, A. W. Thompson and N. R. Moody, Eds. Hoboken, NJ, USA: John Wiley & Sons, Inc., 2013, pp. 1049–1056.

[30] R. J. Walter and W. T. Chandler, "Influence of Gaseous Hydrogen on Metals-Final Report," Canoga Park, CA, Rocketdyne, NASA-CR-124410, 1973.

[31] P. S. Chen, B. Panda, and B. N. Bhat, "Nasa-HR-1, A New Hydrogen Resistant Fe-Ni Based Superalloy," in *Materials*, A. Thompson and N. Moody, Eds. 1994, pp. 1011–1019.

[32] J. A. Harris and M. C. VanWanderham., "Various Mechanical Tests Used to Determine the Susceptibility of Metals to High Pressure Hydrogen Testing," *Hydrog. Embrittlement Testing, STP 543*, vol. 543, no. 1, pp. 198–220, 1972, [Online]. Available: https://www.osti.gov/biblio/4144565.

[33] A. H. Seltzman and S. J. Wukitch, "Nuclear Response of Additive Manufactured GRCop-84 Copper for use in Lower Hybrid Launchers in a Fusion Environment GRCop-84 Material Properties," vol. 02139, no. Mmc, 2020.

[34] J. W. Pyper and C. K. Briggs, "Ortho-para forms of hydrogen, deuterium, and tritium: radiation and self-induced conversion kinetics and equilibria," Livermore, Lawrence Livermore Laboratory, UCRL-52278, 1977.

[35] S. van den Berghe, A. Leenaers, E. Koonen, and L. Sannen, "From High to Low Enriched Uranium Fuel in Research Reactors," in *Advances in Science and Technology*, Oct. 2010, vol. 73, no. 1, pp. 78–90, doi: 10.4028/www.scientific.net/AST.73.78.

[36] J. W. Conant, F. J. Edeskuty, J. E. Huston, and F. V. Thome, "The conversion of para to orthohydrogen in a gamma-ray and neutron radiation field," *Cryogenics (Guildf).*, vol. 15, no. 1, pp. 12–16, Jan. 1975, doi: 10.1016/0011-2275(75)90161-7.

[37] M. Magán, S. Terrón, F. Sordo, F. J. Bermejo, and J. M. Perlado, "Coupled calculation of the influence of the para to ortho conversion in a cryogenic hydrogen moderator," *Phys. Procedia*, vol. 26, no. 1, pp. 211–218, 2012, doi: 10.1016/j.phpro.2012.03.027.

[38] P. R. Gradl, W. Brandsmeier, D. Alberts, B. Walker, and J. A. Schneider, "Manufacturing Process Developments for Large Scale Regeneratively-cooled Channel Wall Rocket Nozzles," 2016.

[39] P. R. Gradl, "Rapid Fabrication Techniques for Liquid Rocket Channel Wall Nozzles," in *52nd AIAA/SAE/ASEE*

Joint Propulsion Conference, Jul. 2016, pp. 1–21, doi: 10.2514/6.2016-4771.

[40] P. Gradl *et al.*, “Robust Metal Additive Manufacturing Process Selection and Development for Aerospace Components,” *J. Mater. Eng. Perform.*, vol. 31, no. 8, pp. 6013–6044, Aug. 2022, doi: 10.1007/s11665-022-06850-0.

[41] P. R. Gradl and C. S. Protz, “Large-scale Channel Wall Nozzle Development Using DED and LWDC Additive Manufacturing Techniques,” in *JANNAF 11th Liquid Propulsion Subcommittee (LPS)*, 2019, pp. 1–34.

[42] P. R. Gradl and C. S. Protz, “Channel Wall Nozzle Manufacturing Technology Advancements for Liquid Rocket Engines Closeout Interface Closeout and Coolant Jacket Coolant Channel Lands (or Ribs) Inner Liner,” in *70th International Astronautical Congress (IAC)*, 2019, pp. 1–16.

[43] M. Le Corre and Z. C. Jones, “Selective Laser Melting Parameter Development of Haynes 230,” *NASA MSFC, Unpbulished Results*, pp. 1–8, 2018.

[44] S. A. Niknam, M. Mortazavi, and D. Li, “Additively manufactured heat exchangers: a review on opportunities and challenges,” *Int. J. Adv. Manuf. Technol.*, vol. 112, no. 3–4, pp. 601–618, Jan. 2021, doi: 10.1007/s00170-020-06372-w.